Supporting Information

Ultranarrow Second-Harmonic Resonances in Hybrid Plasmon-Fiber Cavities

Qi Ai, [*,†] *Lili Gui,* [*,†] *Domenico Paone,* [†] *Bernd Metzger,* [†] *Martin Mayer,* [‡,§] *Ksenia Weber,* [†] *Andreas Fery,* [‡,§,∥] *and Harald Giessen* [*,†]

[†]4th Physics Institute and Research Center SCoPE, University of Stuttgart, Pfaffenwaldring 57, 70569 Stuttgart, Germany

[‡]Leibniz-Institut für Polymer Forschung Dresden e.V. (IPF), Institute of Physical Chemistry and Polymer Physics, Hohe Str. 6, 01069 Dresden, Germany

[§]Cluster of Excellence Center for Advancing Electronics Dresden (cfaed), Technische Universität Dresden, Germany

[∥]Physical Chemistry of Polymeric Materials, Technische Universität Dresden, Germany

Corresponding Author

*E-mail: q.ai@pi4.uni-stuttgart.de, l.gui@pi4.uni-stuttgart.de, h.giessen@pi4.uni-stuttgart.de

1. Characterization of the high-quality gold nanorods we used in the work

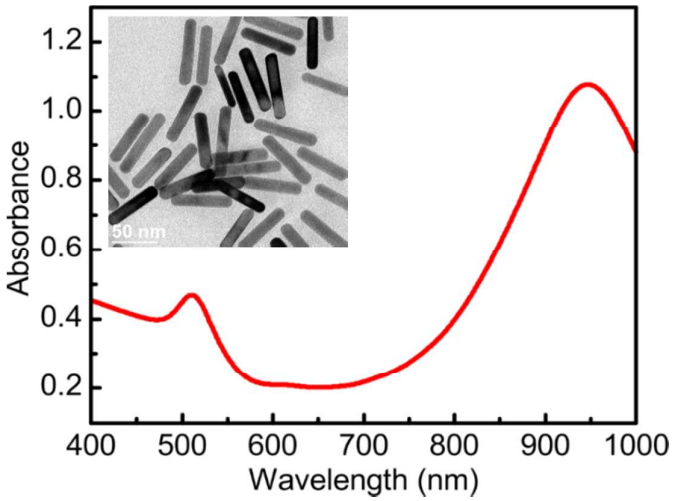

Figure S1. UV-VIS spectrum of gold nanorods in the aqueous solution used in our work. The inset shows a representative transmission electron microscope image.

2. Spectral tunability of hybrid resonance

Efficient coupling between plasmon modes and WGMs which supports a high Q factor at a certain wavelength is obtained by tailoring the diameter of microfibers and aspect ratio of gold nanorods. In other words, the resonant wavelength of the hybrid systems is tunable. Figure S2 illustrates some typical single-band narrow scattering spectra with different resonance positions in the range of 700 nm to 900 nm. The plasmon mode of gold nanorods in aqueous solution exhibits resonances ranging from 873 nm to 1138 nm. It shifts to shorter wavelengths when deposited onto glass substrates or fibers, leaving the upper half exposed to air. The diameters of the different tapered fibers are varied from 1.5 µm to 1.9 µm.

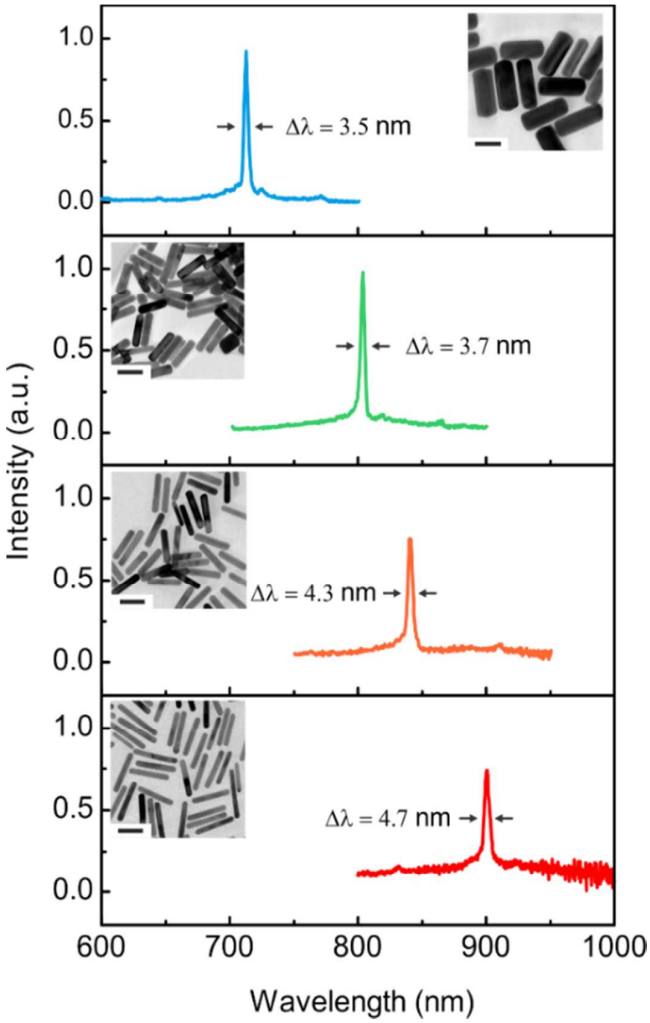

Figure S2. Scattering spectra of coupled systems with different gold nanorod aspect ratios and microfiber diameters. The insets show representative transmission electron microscope images of gold nanorods. Scale bar: 50 nm.

3. Linear scattering spectra of the hybrid plasmon-fiber cavities sensitive to incident angle

The resonance positions of localized surface plasmon modes in metallic nanoparticle systems are usually sensitive to excitation schemes, which is probably due to phase retardation. It holds true also in our coupled systems. Our experimental results suggest that varying the incident angle causes different resonance wavelengths, linewidths, and scattering intensities. As Figure S3 indicates, tuning the incident angle α from 15° to 20° results in red-shifting and narrowing of the resonance for one hybrid cavity. For different gold nanorods on the fiber surface, we also find that the optimum incident angle which leads to the narrowest resonance linewidth and the highest scattering intensity is slightly different.

This difference might be attributed to the varying conditions of the coupled systems, especially the orientation of the gold nanorods deposited on the tapered fibers.

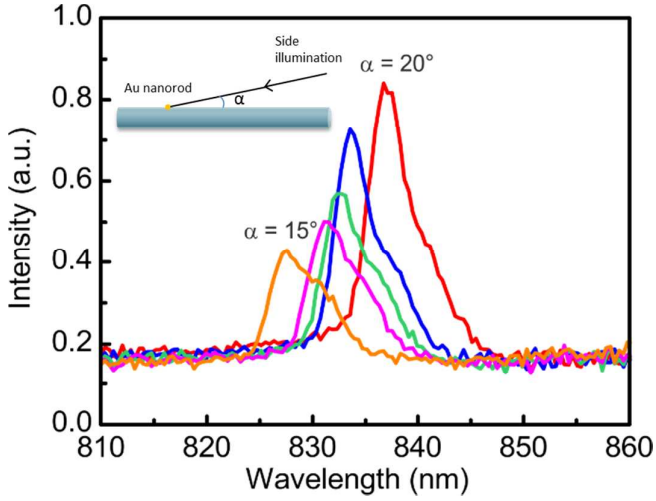

Figure S3. Linear scattering spectra from a gold nanorod on the surface of a microfiber at different incident angles as illustrated by the inset.

4. Scattered laser spectra and second-harmonic emission spectra dependent on different excitation laser wavelengths

In order to demonstrate the SHG efficiency dependence on the excitation wavelength, a series of scattered laser spectra, as well as the second-harmonic emission spectra (with the MPPL baseline subtracted) are presented in Figure S4a and S4b. All these results are the measurement from the hybrid cavity shown in Figures 3a and 3b. Its linear resonance is located at 832.3 nm. We tune the laser center wavelength from 810 nm to 850 nm with 4 nm step size. The scattered laser spectra and corresponding second harmonic emission spectra with the same incident laser are recorded simultaneously (shown in the same colours in Figures S4a and S4b). They are normalized to the same incident power and exposure time. When the excitation wavelength is far away from the linear resonance, scattered laser spectra have only one peak with lower intensity near the excitation wavelength position (see black curve in Figure S4a). Meanwhile, no SHG signal is detectable (see black curve in Figure S4b). As the excitation wavelength is tuned closer to the resonance position, another peak near the resonance appears and grows fast (see sky blue, pink, dark

blue and red curves in Figure S4a). Accordingly, the SH emission has the same trend (see corresponding sky blue, pink, dark blue and red curves in Figure S4b). When we continue to shift the laser spectrum towards longer wavelengths, the intensity of both the scattered laser and SH spectra decreases gradually until they vanish (see green, orange, and purple curves in Figures S4a and S4b). The wavelengths of the SH emission are nearly half of the corresponding scattered laser spectra (it is half the wavelength of the dominating peak close to the hybrid resonance when there are two peaks in the scattered laser spectra). The linewidths of those main peaks in scattered laser spectra are roughly 6 nm. The corresponding SH emission has around 3 nm linewidth, which is smaller than half the linewidth of the fundamental laser[1], giving an additional hint of the ultranarrow linear resonance of our hybrid system. Figures S4c and S4d show the corresponding model results which predict similar features of the scattered laser spectra and second-harmonic emission as a function of the excitation wavelength when compared with our measurement including the overall shape and peak position. There still is some discrepancy in terms of the linewidth mismatch. We suppose that such a disagreement is related to different illumination conditions for laser excitation and white light excitation. The linear scattering was measured by using an unfocused white light source. In Figure S4a and S4b, a focused laser source was utilized, which might change the optical response of the hybrid system (highly sensitive to illumination condition as shown in Figure s3). Our model also employs the extracted parameters by fitting the measured linear scattering.

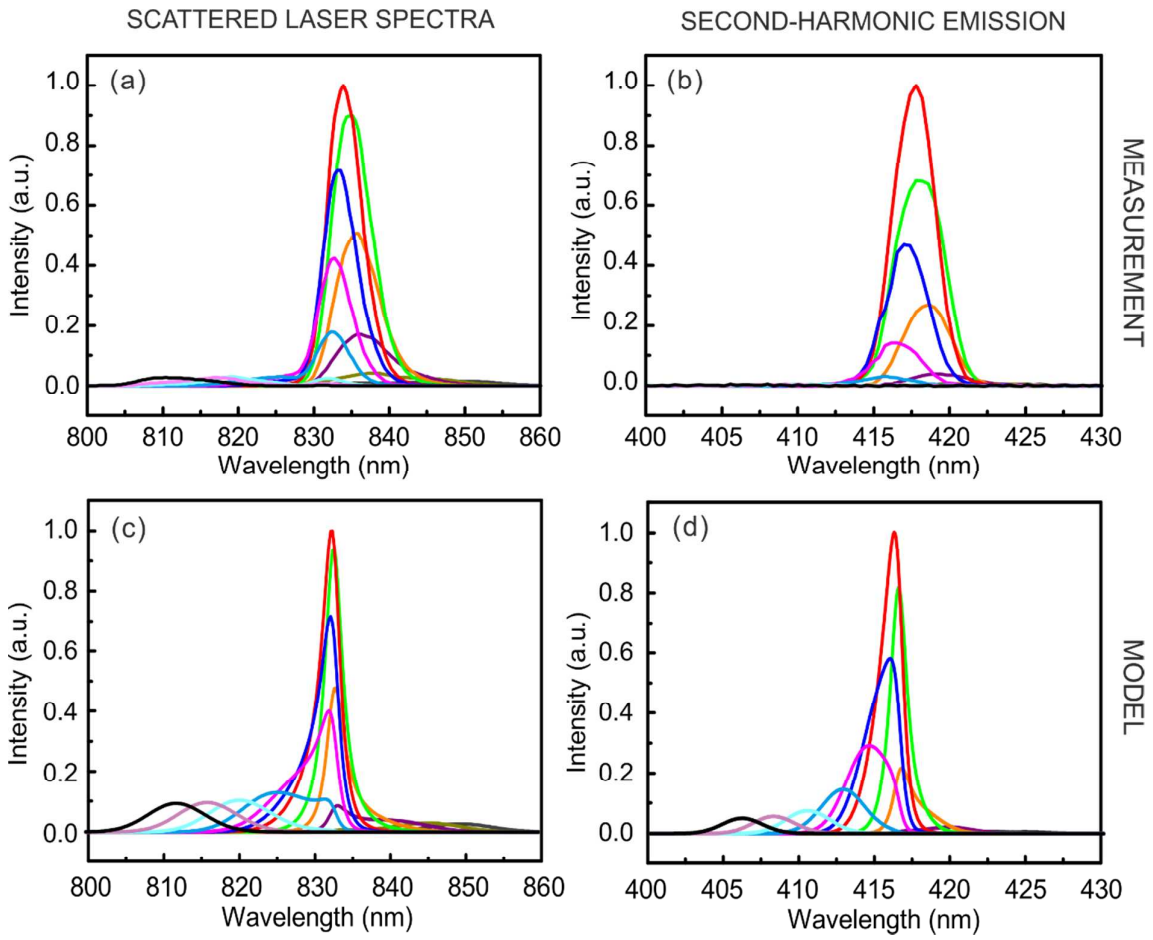

Figure S4. Measured and modelled scattered laser spectra and second-harmonic emission at different excitation laser wavelengths. (a) and (c) are the measured scattered laser spectra, while (b) and (d) are their corresponding second harmonic emission (the spectra with the same excitation wavelength are shown in the same colour in a-d).

5. Fitting parameters for two hybrid systems in Figure 3.

Table S1. Fitting parameters in the anharmonic oscillator model for two hybrid systems in Figure 3.

ω_P(Hz)	γ_P(Hz)	ω_W(Hz)	γ_W(Hz)	κ (Hz^2)
2.37E+15	1.02E+14	2.25E+15	1.77E+13	(2.18E+29)$e^{i(-1.430)}$
2.27E+15	6.87E+13	2.28E+15	2.25E+13	(2.12E+29)$e^{i(-1.469)}$

REFERENCE

(1) Gui, L.; Bagheri, S.; Strohfeldt, N.; Hentschel, M.; Zgrabik, C. M.; Metzger, B.; Linnenbank, H.; Hu, E. L.; Giessen, H. *Nano Lett.* **2016**, *16*, 5708–5713.